AUTONOMOUS DETECTION AND DISAMBIGUATION OF MARTIAN ION TRAILS USING GEOMETRIC SIGNAL PROCESSING TECHNIQUES

Qiutong Jin[1], Ananya Sen Gupta[1], Mirela Kapo[1], Emma Hawk[1], Jasper S. Halekas[2]

[1]Department of Electrical and Computer Engineering, University of Iowa
[2]Department of Physics and Astronomy, University of Iowa

ABSTRACT

We propose a novel "big data" application of geometric feature extraction techniques to autonomously identify and track the temporal evolution of charged particle trails in the Martian ionosphere. Specifically, we propose a Radon-transform extension to the geometric distance transform to algorithmically isolate potentially overlapping trail features in energy spectrograms. Our methods seek to connect large-scale statistical analysis with individual case studies and thus provide the computational framework or connecting theoretical models with potential terabytes of remote sensing data. Based on individual ion populations as the basic unit of observation, we provide data-driven results of applying our method over representative energy spectrograms generated from the NASA Mars Atmosphere and Volatile Evolution (MAVEN) mission data from the Solar Wind Ion Analyzer (SWIA) instrument.

Index terms— morphological signal processing, distance transform, radon transform, feature extraction.

1. INTRODUCTION

The overarching objective of this work is to automatically track, disentangle, and quantify the complex trajectories of Martian ions [1-5], at the granularity of individual ion populations, in the Martian atmosphere across terabytes of existing (and growing) data from the MAVEN mission. The science application of our proposed techniques is to observe the evolution dynamics, dependencies and interactions of individual ion populations at different scales of time, space, energy and other factors, such as impact of the solar wind on Martian atmospheric loss. In the larger context, such automated computational techniques are deeply needed to complement manual case studies and enable large-scale quantitative determination of a fundamental science question: *How did Mars lose its atmosphere and water?*

1.1 Background motivation

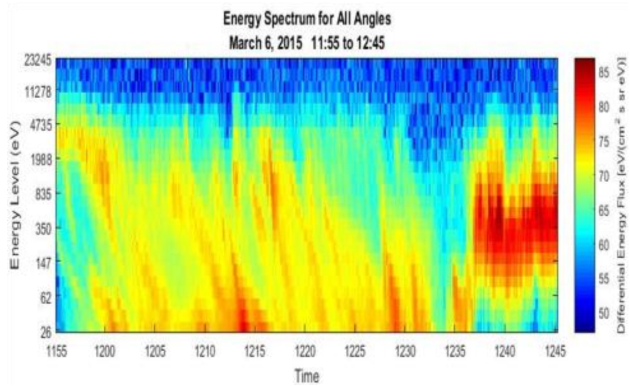

Figure 1. Energy spectrogram showing the integrated differential energy flux $\psi(e, t) = \int \psi(e, t, \phi, \theta)\, d\theta d\phi$.

Figure 1 illustrates a typical energy spectrogram where the color axis is given by the differential energy flux $\psi\,(\cdot)$ that measures the rate of transition of different ion populations as a function of given time (t) and energy (e), integrated across multiple solid angles defined by the azimuthal and polar angles (θ and ϕ), respectively. SWIA data typically measures $\psi(\cdot)$ across a unique grid of (θ, ϕ), and therefore, offers resolution of distinct ion escape pathways that can occupy different positions in space, while occupying the same energy levels at the same time [4]. However, due to demands on human precision and personnel time, such angle-specific trail studies, as well as studies connecting potentially overlapping multi-dimensional trails spanning different (θ, ϕ) trajectories have never been done at a large scale within the space science community. Given that millions, potentially billions of such trails exist over the spatial-temporal span of the multi-year MAVEN mission, this raises a classic "big data" challenge.

The compelling automation and signal processing challenges then rest in isolating these ion trails, which manifest as continuous, albeit noisy trajectories of ion populations across the differential energy flux spectra, denoted as $\psi(e, t, \phi, \theta)$, and thread potentially continuous trajectories that overlap in the (θ, ϕ) space.

1.2 Related work

The primary hardship of automating individual ion population studies is lack of geometric measures to computationally identify, separate and track potentially overlapping ion escape processes across distinct portions of velocity phase space (refer figure 2 (a)).

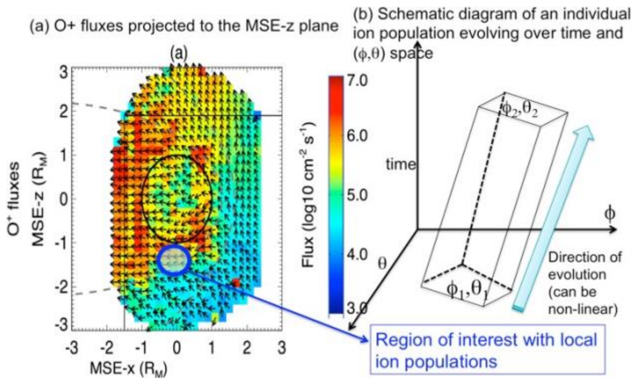

Figure 2. (a) O+ fluxes projected to the MSE (x-z) plane, which are averaged over the y-direction [5]. The arrows show flux and velocity directions, while the colors label the magnitudes. (b) Schematic diagram of how an individual ion population within a local region of interest might evolve over time, spanning a range of polar and azimuthal angles.

As such, large-scale studies on maven datasets have been limited to mostly correlation-based or otherwise purely statistical analysis [1-5] of data accumulated across thousands of ion escape processes. As such, no effort has been made towards connecting these aggregated maps (e.g. Figure 2(a)) to the evolution of individual ion populations (figure 2(b)) that constitute these escape processes across multiple scales of space, energy and time. On the other hand, within the last few decades, the geometric and morphological signal processing community has witnessed a burgeoning of feature extraction and automation techniques (e.g. [6-16] and references therein) that are highly applicable to big data scenarios such as this interdisciplinary and high-impact application.

2. TECHNICAL APPROACH

2.1 Key contributions

In this work, we report the first steps towards developing a "computational microscope with tunable focus" that harness popular and recently proposed geometric signal processing techniques [14-16, 20] to enable this large-scale automated study across terabytes of SWIA data from the maven mission. Specifically, we propose a two-pronged approach to isolating Martian ion trails using the well-known Radon transform [14,15], as well as the geometric distance transform [16]. The Radon transform approach is similar in principle to the Ridge transform technique [20] recently proposed for isolating high-energy plasmaspheric events within the earth's Van Allen radiation belts. The significant difference between the Ridge transform method and our Radon-based methodology here is that the ion trail features, unlike the features selected in [20], are highly non-linear and significantly more prone to background noises.

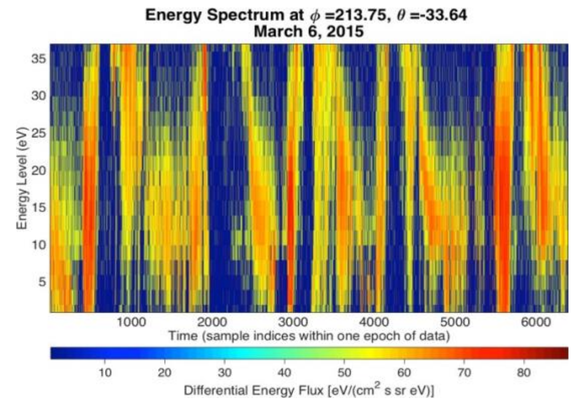

Figure 3: original spectrogram $\psi(e, t, \phi, \theta)$ obtained at (θ = −33.64°, ϕ = 213.75°) over 24 hours (00:00 – 23:59 UTC of data).

Therefore, instead of applying the Ridge transform directly, we use the geometric distance transform [16,17] as a first step to isolate the main ionic trails and their spines and then apply the Ridge transform locally to detect microstructure within the trail morphology as applicable.

We provide relevant data-driven results and related discussion within the context of our technical approach in each step.

2.2 Step 1: Detecting trail features using the Distance Transform

To achieve our data analysis goal for detecting and disambiguating trails against the noisy background, we employ the distance transform, which is a well-known morphological technique [16,17], to isolate the persistent geometric features within the original image. As a case study we will illustrate our method over a 24-hour span of data for fixed (θ,ϕ) as given in Figure 3. In our implementation, the distance transform is an Euclidean distance operator applied to the gray-scale version of the spectrogram ψ (e, t, ϕ, θ). Figure 4(b) shows the result of applying the distance transform (DT) to the spectral image in Figure 3.

An alternative method is to employ the singular value decomposition (SVD) transform, which is a well-developed signal processing technique that could remove noises effectively. However, by comparing the results obtained from distance transform (Figure 4(b)) and SVD transform (Figure 4(c)), we find that distance transform works better in noise removal.

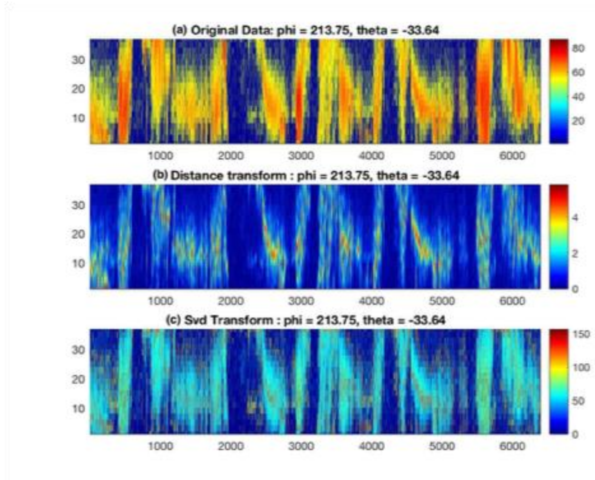

Figure 4: Original spectrogram (Figure 4(a)). Distance Transform of the original spectrogram (Figure 4(b)). SVD transform of the original spectrogram (Figure 4(c)).

2.3 Step 2: Detecting trails from the distance transform using binary thresholding and morphological operations

We threshold the DT image to a geometric distance $\tau = 1$ to create a binary mask of the original spectrum. This creates clearer noise-robust feature boundary to enable precise trail detection and trail isolation in subsequent steps. We select the value of $\tau = 1$ based on extensive empirical observations across all available 64 combinations of (θ, ϕ). We further adopt morphological "open" operations [18] to remove small holes inside each trail.

After the binary feature extraction, the extracted trails are separated by gaps with each other. To detect individual trails, we employ a connectivity search [19] over the binary features and isolate any connected trail as an individual ion escape population. By mapping the isolated binary trails back to the original spectrogram in figure 3, we derive the final spectral trajectories of each ion population. Figure 5 shows the autonomously isolated trail trajectory of the second ion population in figure 3.

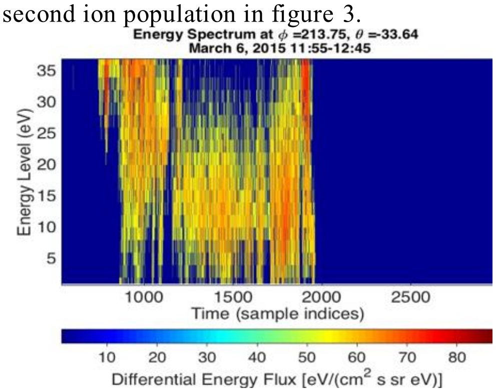

Figure 5: Ion trail isolated from Figure 3.

2.5 Step 4: Finding the spines of each detected ion trail

The "spine" of each ion trail within the spectrogram is defined as the temporal trace of the highest flux activity within the trail feature. Mathematically, this may be expressed as:

$$\psi_s(e(t), \phi, \theta) = \arg\max_e \psi(e, t, \phi, \theta)$$

Where $\psi_s(e(t), \phi, \theta)$ denotes the differential energy flux across the temporal trace $e(t)$ for a given spatial location, i.e., for a particular (θ, ϕ).

Accordingly, $\psi_s(e(t), \phi, \theta)$ can be obtained by finding the index of the maximum pixel of each column in trails found in original spectrogram (figure 3). By plotting these indices versus time, we autonomously generate the spines of original spectrogram in figure 3.

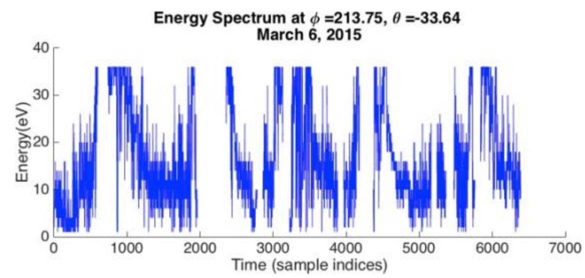

Figure 6: Spines of the original spectrogram.

2.6 Extracting microstructure within individual trails using Ridge transform.

We note that the trails isolated in the 24-hour case study are still extracted at the micro-level, i.e., the extracted features, including trail spines exhibit significant perturbations over energy across time even for a single (θ, ϕ) combination. To extract trail microstructure over finer resolution in time, the distance transform method was not found to be adequate, since the geometric threshold $\tau = 1$ was robust only across longer scales of time. Furthermore, when two trails overlap over time, the DT method was inadequate to disambiguate the trails. To accommodate this dilemma, we first isolate the macro trail features using steps 1-4 outlined above over longer ranges to isolate the major trail activity and then employ the Ridge transform [20], recently proposed to identify locally linear spectral features in the Earth's Van Allen radiation belts, to identify potentially overlapped trail microstructure. In synopsis, the Ridge transform employs the well-known Radon transform [14,15] to detect and trace locally linear spectral elements by isolating angles of projection for which the spectral image accumulates significant energy. However, unlike the original application of the Ridge transform, ion trails may exhibit multiple peak maxima in the Radon domain, each corresponds to significant features within the trail microstructure. In particular, potentially overlapped trails will manifest as separate high peaks in the Radon domain. Figure 7 demonstrates such a case. We detect the spectral features of each high peak in the Radon domain along a sliding rectangular window to disambiguate locally linear features ("ridges"). Therefore, applying the Ridge transform across potentially multiple local maxima helps us disambiguate potentially cross-crossed trails as shown in Figure 7.

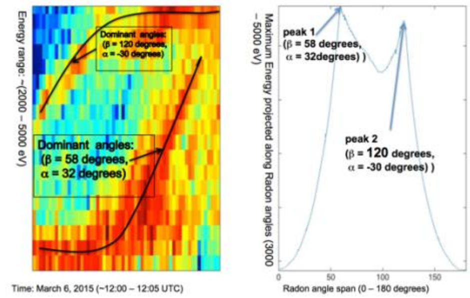

Figure 7: Disambiguating trail microstructure by employing the Ridge transform across multiple peaks in the Radon domain.

2.7 Connecting ion trails across different polar and azimuthal angles

Our methodology so far has focused on the spectral image for a given (θ, ϕ) combination. In practice, an ion trail can span across multiple ranges of (θ, ϕ). To resolve this, we provide an alternative visualization of the ion trails in the (θ, ϕ) domain instead of the energy spectral (e, t) domain. Figure 7 shows a temporal snapshot of the total energy spectrogram given in figure 1, where the differential energy flux is integrated across all energy levels and the temporal window chosen is (11:55-12:45 UTC) for every (θ, ϕ) combination. Each peak in this (θ, ϕ) domain represents the cumulative flux of ion trails that share connected angular coordinates. The evolution of each peak can spin multiple (θ, ϕ) combinations, which can then be mapped back to ion trails identified in the (e, t)-domain using techniques discussed in previous sections.

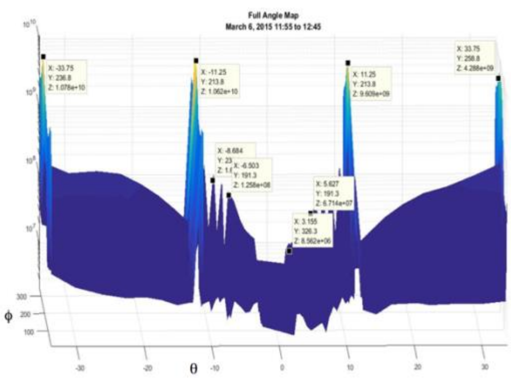

Figure 8: Location ion trails across the (θ, ϕ) domain.

2.8 Detecting trails from SVD transform

We perform the same analysis (Section 2.2-2.5) using SVD transform and could also isolate trails from the original spectrogram (Figure 9).

By comparing Figure 9 with Figure 5 (Ion trail isolated from DT), we can clearly see that some parts (~900-1200) are missing in the SVD one. In other word, detecting trails using SVD transform may cause the loss of some information. While distance transform does not have this concern.

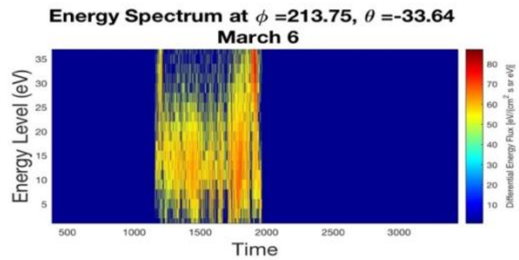

Figure 9: One trail detected using SVD transform and techniques mentioned in previous sections

3. RESULTS AND DISCUSSION

Wherever applicable, we have provided relevant data-driven results and related discussion within the context of our technical approach in each step of Section 2. As a representative summary of our techniques, we provide a break-up of the energy spectra along five main ion populations isolated in the (θ, ϕ) domain, in a 3-hour case study for the same date (March 6, 2015), which offers a half-way scale between the short (11:55-12:45 UTC) and long (24 hours) observation windows. Results presented here are representative of typical case studies and future directions include large-scale study of ion trails across potentially terabytes of MAVEN mission date using the techniques proposed in this work.

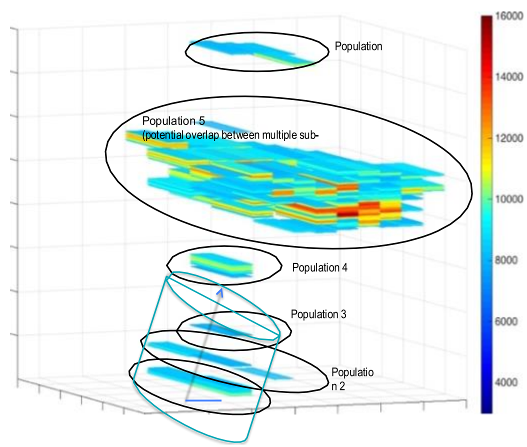

Figure 10: autonomously isolated ion populations showing distinct populations with one (population 5) consisting of potentially overlapped sub-populations, and three populations (1-3) potentially connected by the topological similarity across ~3 hours of SWIA data recorded on March 6, 2015. Each ion population shown exhibits color proportional to differential energy flux integrated over all energy levels and observed continuously over ~2 minutes (to eliminate noise). To identify salient topological boundaries, we isolate the ion populations that exhibit integrated energy greater than 8000 eV/ (cm^2 eV), which serves as a tunable threshold to discover salient topological features of dominant ion populations within a local region in phase space.

4. REFERENCES

[1] Jakosky, B. M., and R. J. Phillips, Mars' volatile and climate history, Nature, 412(6), 237–244, 2001.

[2] Dubinin, E., M. Fraenz, A. Fedorov, R. Lundin, N. Edberg, F. Duru, and O. Vaisberg, Ion Energization and Escape on Mars and Venus, Space Sci Rev, 162(1), 173–211, doi:10.1007/s11214-011-9831-7, 2011.

[3] Halekas, J.S. et al. (2015), Time-dispersed ion signatures observed in the Martian magnetosphere by MAVEN, Geophys. Res. Lett., 2015.

[4] Halekas, J. S., et al. "The solar wind ion analyzer for MAVEN." Space Science Reviews: 1-27, 2013.

[5] Dong., Y., et al. Strong plume fluxes observed at Mars by MAVEN: An important planetary ion escape channel, Geophys. Res Lett., 2015.

[6] Meyer, Fernand. "Topographic distance and watershed lines." Signal processing 38.1: 113-125, 1994.

[7] M. Nakahara, "Geometry, topology and physics", CRC Press, 2003.

[8] C. Nash, S. Sen, "Topology and geometry for physicists", Courier Corporation, 2013.

[9] Dougherty, E. R., Lotufo, R. A., & The International Society for Optical Engineering SPIE. Hands-on morphological image processing (Vol. 71). Bellingham: SPIE press, 2003.

[10] Bobin, J., Starck, J. L., Fadili, J. M., Moudden, Y., & Donoho, D. L., Morphological component analysis: An adaptive thresholding strategy. Image Processing, IEEE Transactions on, 16(11), 2675-2681, 2007.

[11] Maragos, P., & Ziff, R. D. Threshold superposition in morphological image analysis systems. Pattern Analysis and Machine Intelligence, IEEE Transactions on, 12(5), 498-504, 1990.

[12] Hasan, Y. Y., & Karam, L. J. Morphological text extraction from images. IEEE transactions on image processing: a publication of the IEEE Signal Processing Society, 9(11), 1978-1983, 1999.

[13] Nikias, C. L., & Mendel, J. M. (1993). Signal processing with higher-order spectra. IEEE Signal processing magazine, 10(3), 10-37.

[14] Deans, S. R. The Radon transform and some of its applications. Courier Corporation, 2007.

[15] Beylkin, G., Imaging of discontinuities in the inverse scattering problem by inversion of a causal generalized Radon transform. Journal of Mathematical Physics, 26(1), 99-108, 1985.

[16] Fabbri, Ricardo, Luciano Da F. Costa, Julio C. Torelli, and Odemir M. Bruno. "2D Euclidean distance transform algorithms: A comparative survey." ACM Computing Surveys (CSUR) 40, no. 1 2008.

[17] Matlab implementation of grayscale distance transform: https://www.mathworks.com/help/images/ref/graydist.html

[18] Matlab implementation of morphological opening operation: https://www.mathworks.com/help/images/ref/bwareaopen.html

[19] Matlab implementation of detetermining connectivity between binary features: https://www.mathworks.com/help/images/ref/bwconncomp.html

[20] Sen Gupta, Ananya, Craig Kletzing, Robin Howk, William Kurth, and Morgan Matheny. "Automated identification and shape analysis of chorus elements in the Van Allen radiation belts." Journal of Geophysical Research: Space Physics 122, no. 12 (2017).